Science Advances
AAAS

advances.sciencemag.org/cgi/content/full/6/13/eaay7608/DC1

Supplementary Materials for

Bioenergetic-active materials enhance tissue regeneration by modulating cellular metabolic state

Haoming Liu, Yingying Du, Jean-Philippe St-Pierre, Mads S. Bergholt, Hélène Autefage, Jianglin Wang, Mingle Cai, Gaojie Yang, Molly M. Stevens*, Shengmin Zhang*

*Corresponding author. Email: m.stevens@imperial.ac.uk (M.M.S.); smzhang@hust.edu.cn (S.Z.)

Published 25 March 2020, *Sci. Adv.* **6**, eaay7608 (2020)
DOI: 10.1126/sciadv.aay7608

This PDF file includes:

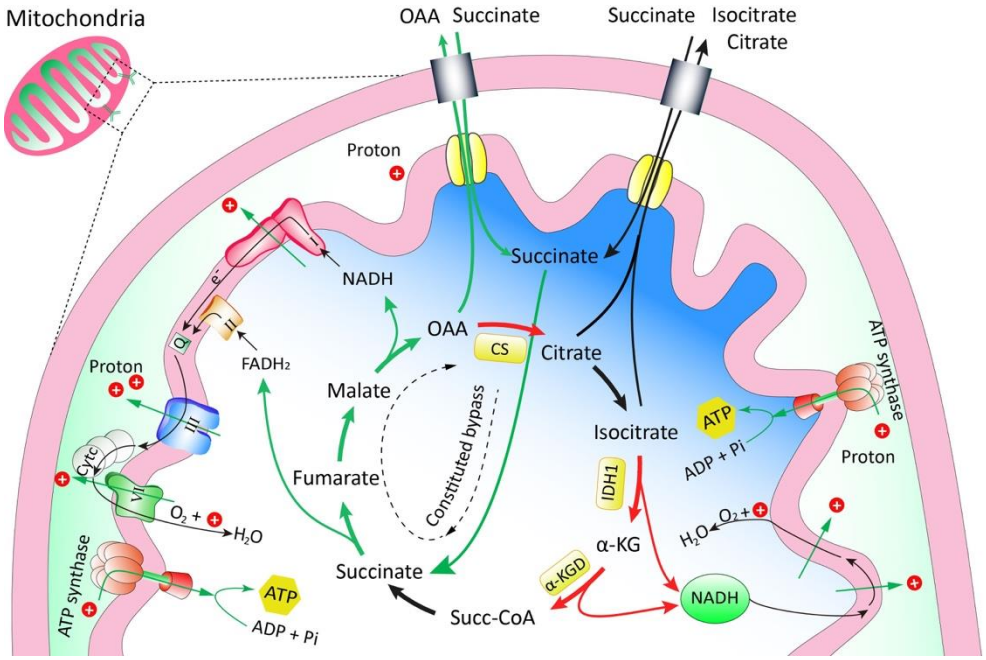

Fig. S1. Schematic illustration of the establishment of a bypass in the TCA cycle by uptake of succinate resulting from the hydrolysis of degradation fragments. This bypass is hypothesized to raise the metabolic state (processes indicated with dotted arrows) and enhance the mitochondrial membrane potential (transferring electropositive protons out through the inner membrane) in a degradation-mediated manner.

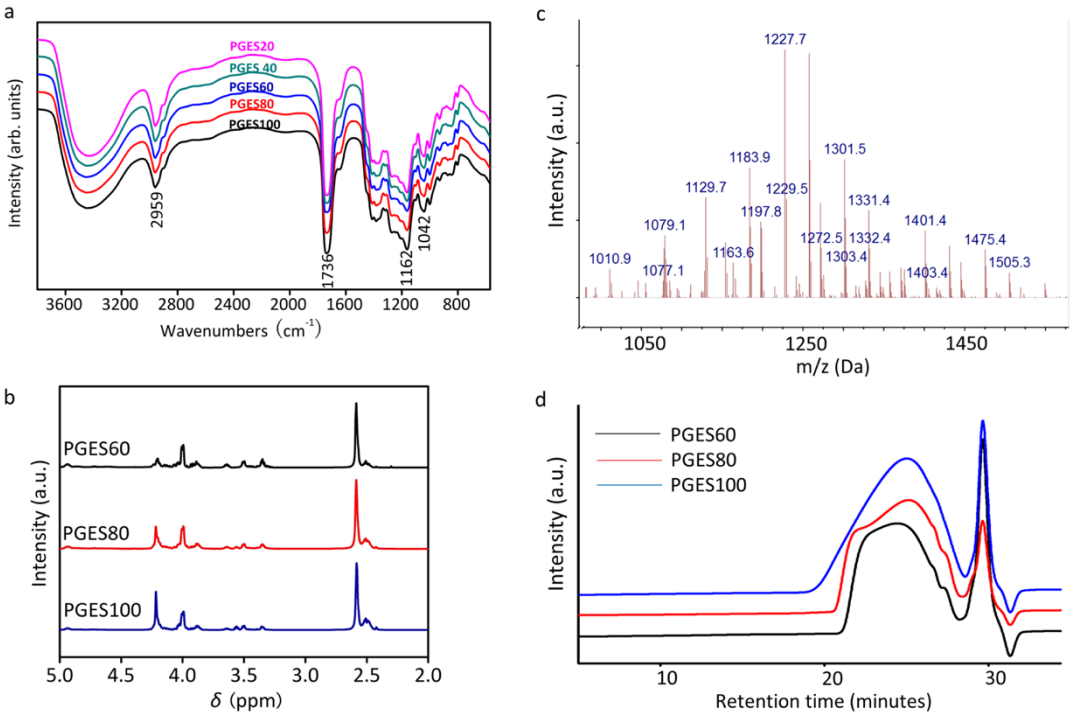

Fig. S2. Spectrum characterization for the prepolymers synthesized in this study before cross-linking. (**a**) Fourier transform infrared spectroscopy characterization of the different PGES prepolymers. All the samples demonstrated strong carbonyl stretching vibration at around 1736 cm^{-1} from the ester group of the prepolymers. Two strong peaks at 1162 cm^{-1} and 1042 cm^{-1} assigned to C-O-C stretching vibration also confirmed the prepolymers structure. The asymmetric and symmetric stretching vibrations of the methylene -CH_2- group in the backbone were shown at 2959 cm^{-1} and 2850 cm^{-1}, respectively. With increasing glycerol incorporation from sample PGES20 to PGES100, the broad absorption from 2800 cm^{-1} to 3600 cm^{-1} assigned to -OH group in glycerol and terminal carboxylic group exhibits a stronger signal. (**b**) ^{1}H NMR spectra for the different PGES prepolymers. (**c**) Mass spectrum for the molecular weight of a representative prepolymer (PGES80) presenting a normal distribution, with a number average molecular weight of about 1,200 kDa. (**d**) Gel permeation chromatography for different PGES prepolymers.

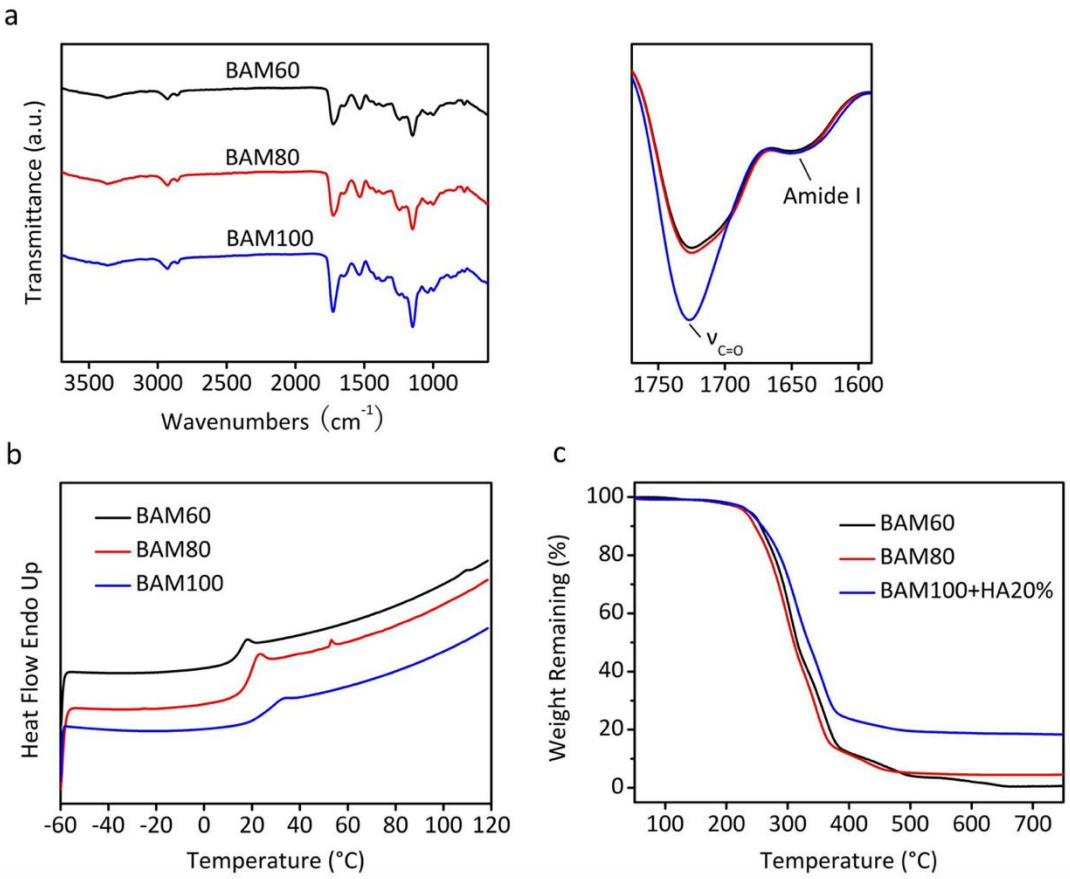

Fig. S3. Spectrum characterization for the BAM polymers after cross-linking. (**a**) Fourier transform Infrared spectroscopy, (**b**) differential scanning calorimetry, and (**c**) thermogravimetric analysis for polymers BAM60, BAM80, and BAM100 composited with 20% (wt) HA. The urethane group in the polymer was confirmed by peaks at around 3340 cm^{-1} and 1640 cm^{-1}, which were assigned to the imide -NH- stretching and bending vibration from the urethane groups, respectively. All of the polymers showed typical glass transition temperatures attributed to soft segment. The glass transition temperatures increased with increasing glycerol molar ratio in the soft segment, from 14.42 ˚C for BAM60 to 24.79 ˚C for BAM100, because molecule segment flexibility was restricted by glycerol crosslinking. The decomposition temperature of the polymers varies slightly from 350 ˚C to 360 ˚C. The compounds lost more than 95% of mass at the temperature from 250 ˚C to 390 ˚C.

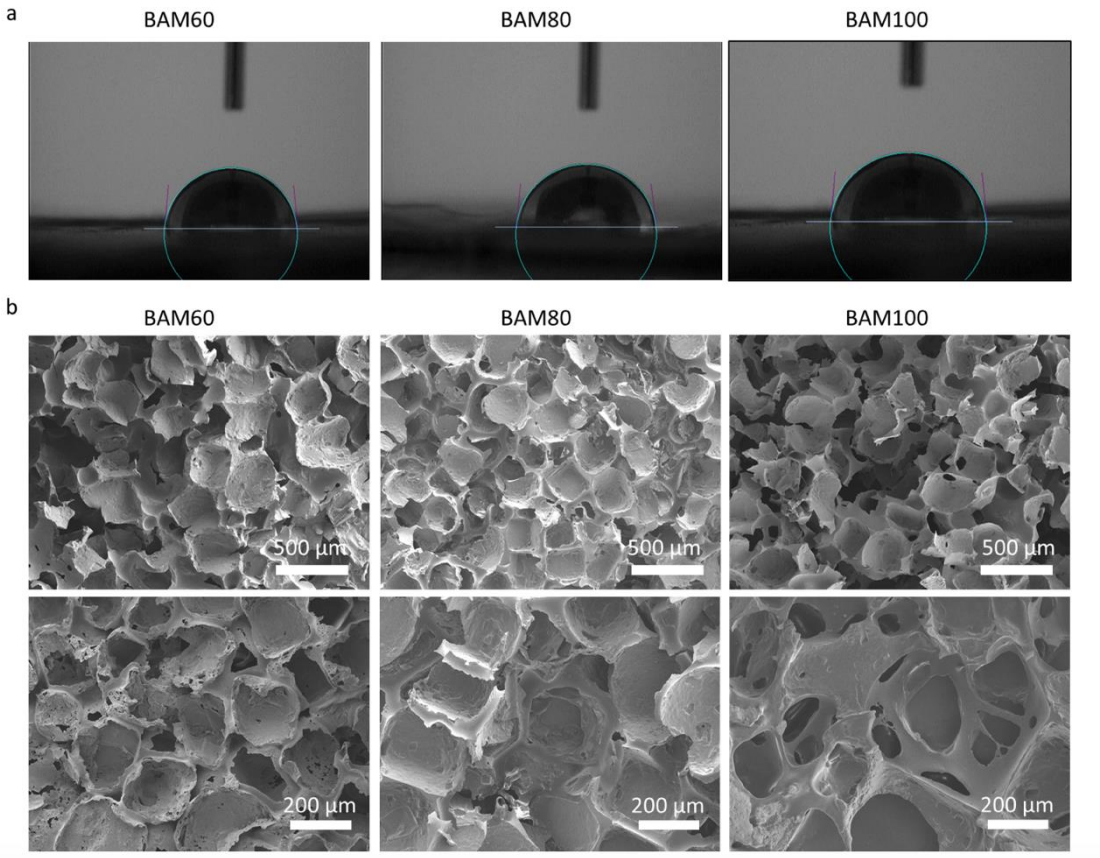

Fig. S4. Hydrophilicity and morphology characterization of BAM. (**a**) Contact angle measurements of the BAM60, BAM80 and BAM100 polymers. The results show that all samples had a good hydrophilic property with the contact angle less than 90°. The hydrophilic property was increased with an increase of the glycerol content. (**b**) SEM images of porous BAM60, BAM80, and BAM100 scaffolds showing the presence of interconnected pores in the scaffolds. The SEM image for BAM100 at lower magnification was taken in the same area as shown in Fig. **1c**.

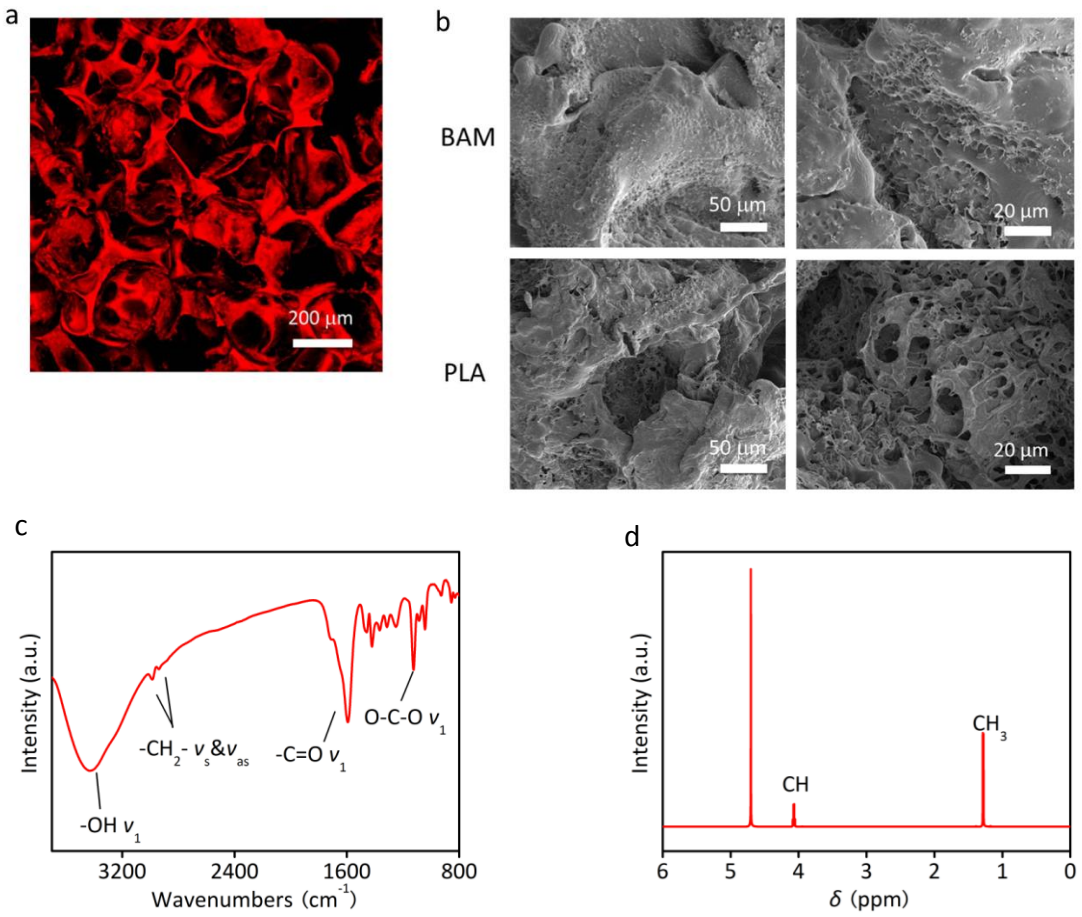

Fig. S5. In vitro degradation of BAM and PLA scaffolds in PBS. (**a**) Fluorescence image of a representative BAM scaffold obtained by confocal laser scanning microscopy. The scaffold was stained with rhodamine B, before immersion in PBS for 2 weeks. (**b**) SEM images of BAM and PLA scaffolds after 12 weeks degradation in PBS, showing that the BAM scaffold maintained the porous structure. 0.1-2 µm pores on the surface indicate that the BAM may undergo a surface corrosion mechanism. (**c**) FT-IR and (**d**) ^{1}H NMR spectra confirming the presence of lactic acid in the degradation solution of PLA scaffold. Absorption peaks at around 2950 cm^{-1} (-CH_2-) & 1120 cm^{-1} (O-C-O) in FT-IR spectra and absorption peaks between 1.2 ppm (-CH_3) and 4.1 ppm (-C-H) in ^{1}H NMR spectra are attributed to the lactate molecule.

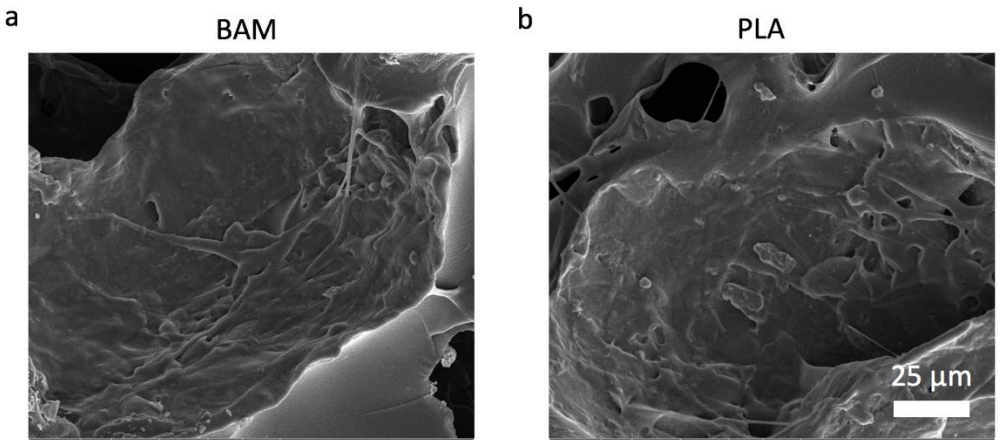

Fig. S6. SEM image of rMSCs. The cells were seeded on BAM (**a**) and PLA (**b**) scaffolds, and incubated in DMEM for 3 days. After that cells were fixed, dehydrated, gold- sprayed and imaged by SEM.

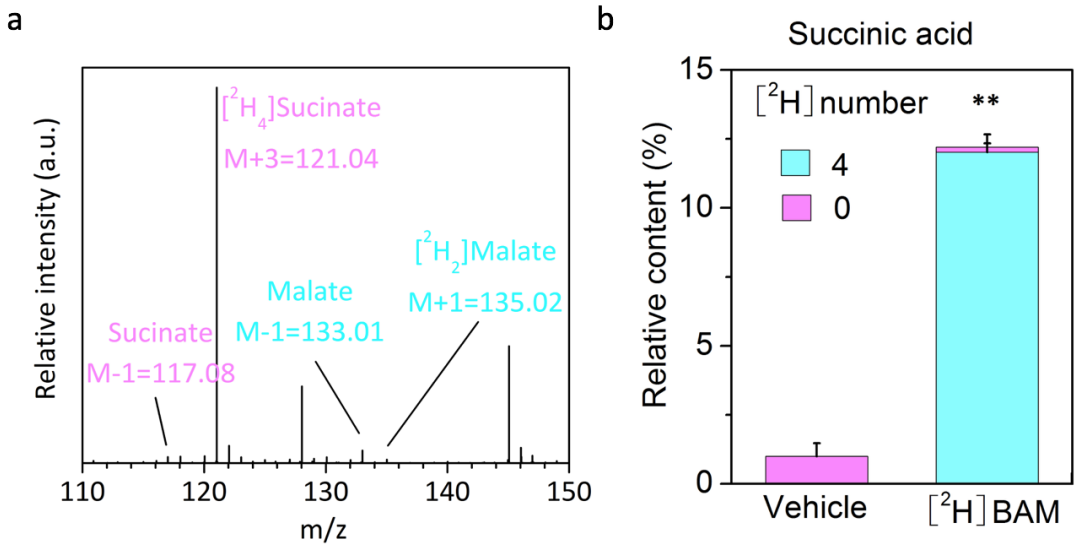

Fig. S7. LC-MS analysis for the succinate content in rMSCs. (**a**) Mass spectrum of the cell lysate after the cells were incubated with deuterated BAM degradation fragments ([^{2}H$_4$]BAM) for 6 h. The deuterated succinate (m/z = 121) and deuterated malate (m/z = 135) were detected in the spectrum, indicating that BAM fragments can be internalized by rMSCs. (**b**) Quantitative determination of deuterated [^{2}H$_4$]succinate and unlabeled succinate in deuterated BAM degradation fragments treated cells ([^{2}H$_4$]BAM) and untreated cells (Vehicle). The results showed that treatment of rMSCs with deuterated BAM significantly enhanced [^{2}H$_4$]succinate level in the cell lysates, compared to unlabeled succinate level in vehicle group. Results represent means ± standard deviation (n = 3 cell cultures per group). Statistical analysis: unpaired two-tailed Student's t test. ∗ $p < 0.05$, significant differences versus vehicle group.

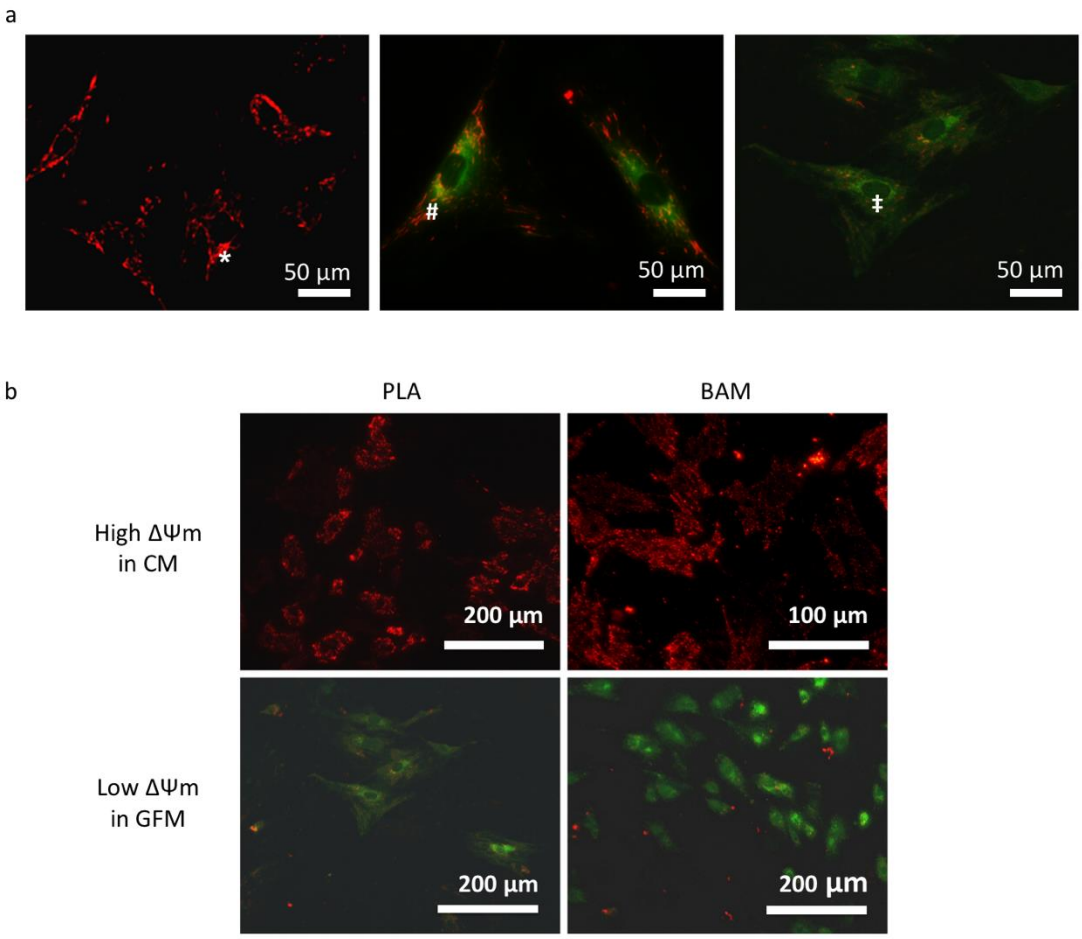

Fig. S8. Fluorescent images of JC-1 staining for mitochondrial membrane potential. (**a**) Fluorescent images of JC-1 staining for mitochondrial membrane potential in rMSCs with different metabolism level. The cells were maintained in high glucose DMEM (left), or 60 min (middle) or 12 hours (right) after treatment with glucose-free medium, respectively, before being stained with JC-1 and examined using a fluorescent microscopy. * indicates cells with high ΔΨm and aggregated JC-1, # indicates cells with reduced ΔΨm, ‡ indicates cells with low ΔΨm and free JC-1. (**b**) Fluorescent images of JC-1 staining for the mitochondrial membrane potential in rMSCs cultured in normal culture medium (CM, upper) and glucose-free medium (GFM, bottom) supplemented with degradation fragments from the PLA or BAM groups.

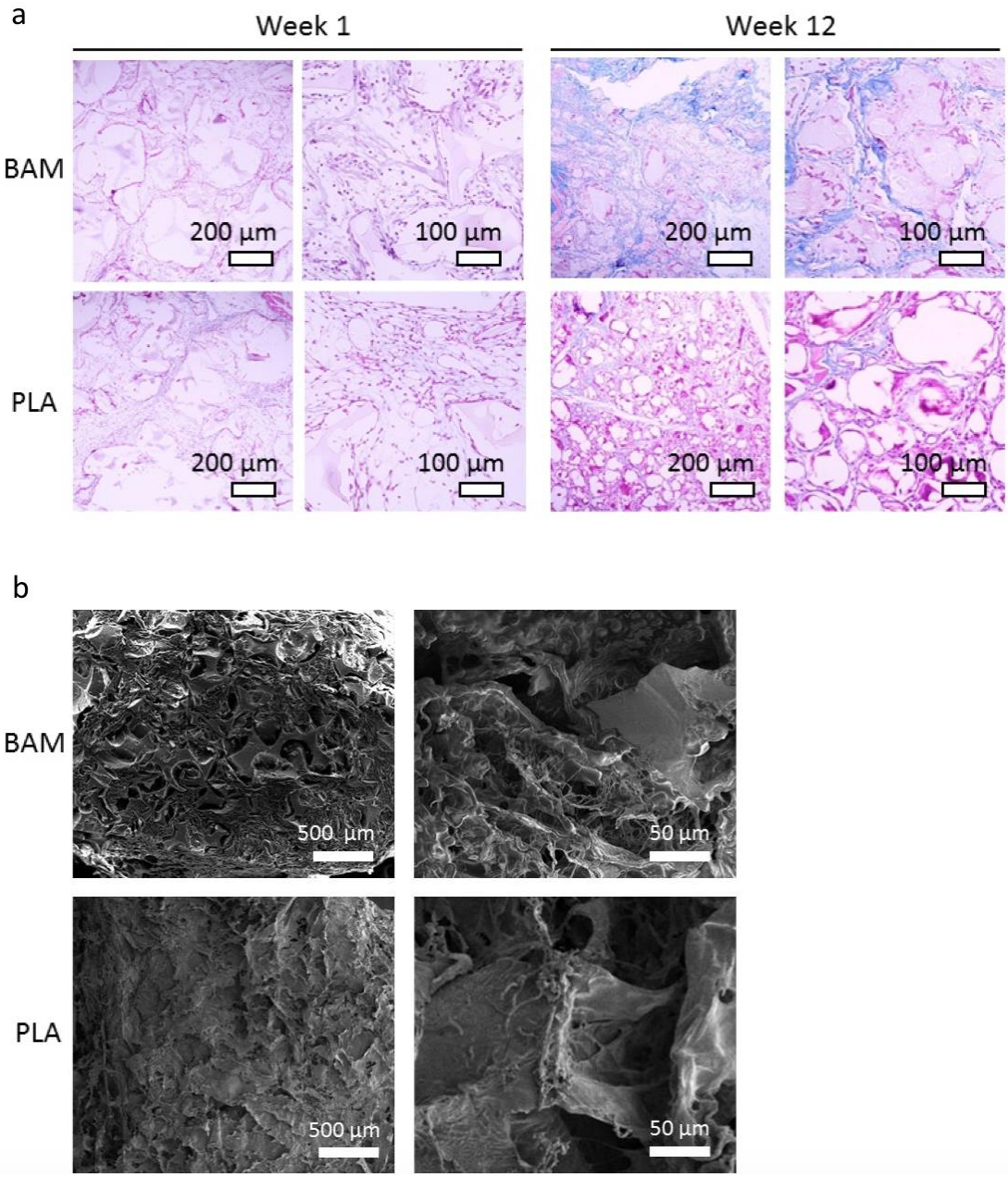

Fig. S9. Masson's trichrome staining and SEM images of BAM and PLA scaffolds after subcutaneous implantation. (**a**) Masson's trichrome staining of histological sections from BAM and PLA scaffolds retrieved 1 week and 12 weeks after subcutaneous implantation in mice. (**b**) SEM images of tissue ingrowth in the porous BAM and PLA scaffolds retrieved 12 weeks after subcutaneous implantation in mice.

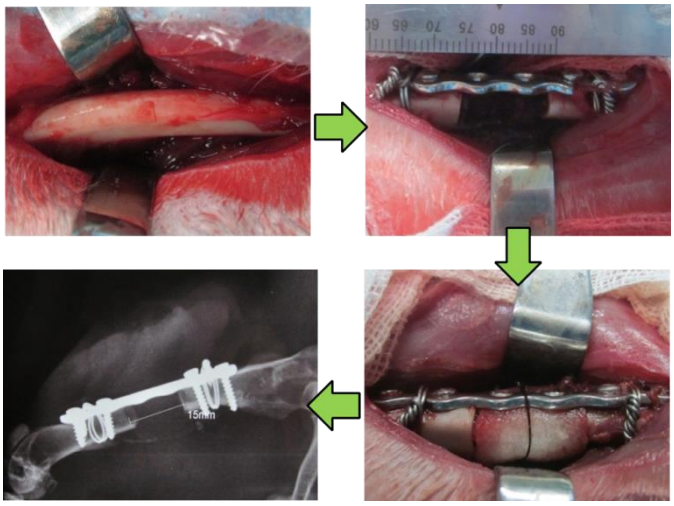

Fig. S10. The construction of a critical-sized segment defect in rabbit femur. The bone is exposed and a 15 mm segment of bone is removed. The two ends are fixed with screws and plate. The scaffolds are positioned in the defect and attached with wire. X-ray imaging confirmed the defects immediately after the surgery, showing that the implanted scaffold is nonopaque to X-ray. Photo Credit: Haoming Liu, Huazhong University of Science and Technology.

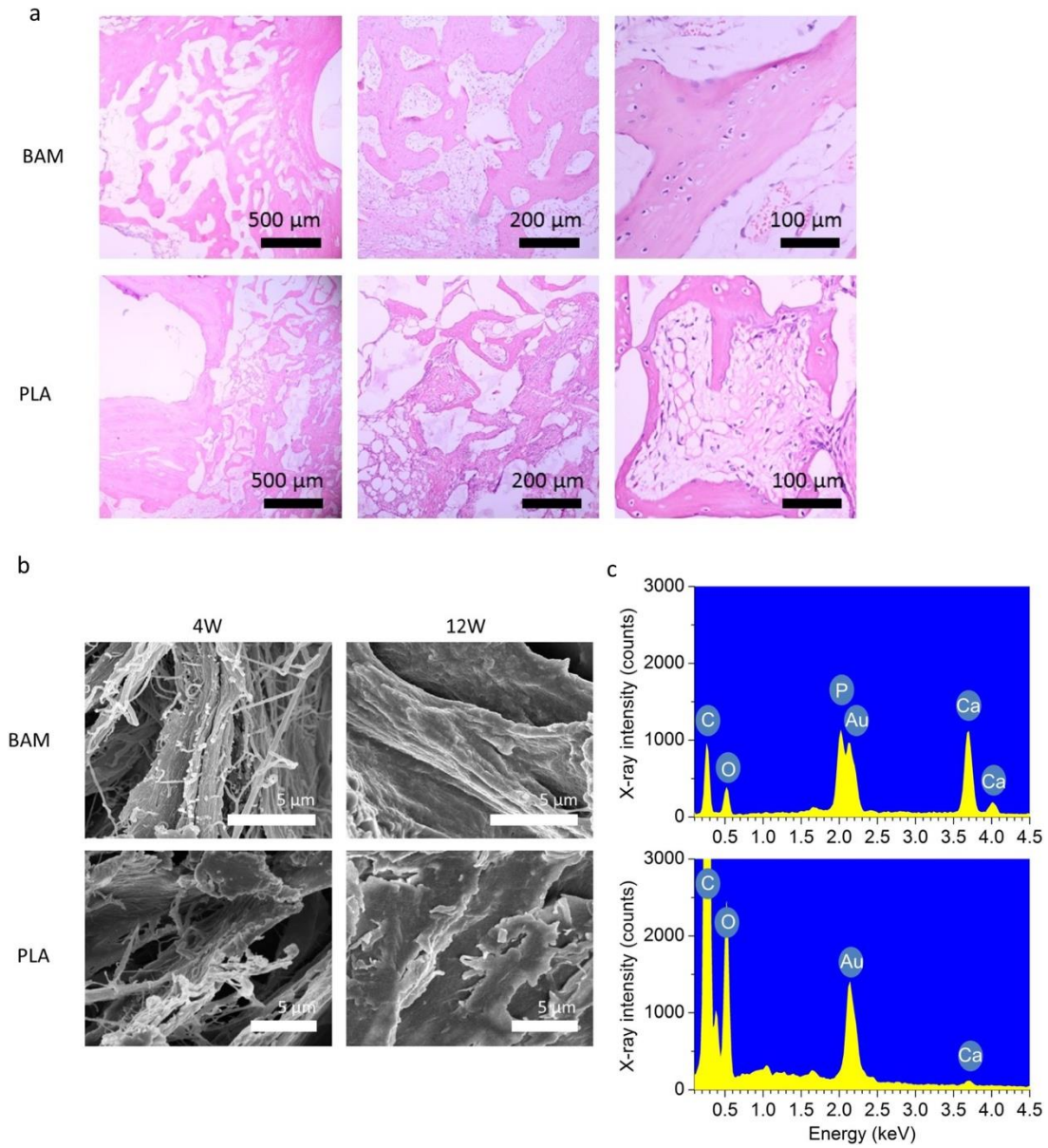

Fig. S11. H&E staining, SEM, and EDX elemental scanning for the analysis of bone regeneration. (**a**) Hematoxylin & eosin staining of histological sections of bone ingrowth in the porous BAM and PLA retrieved from rabbit femurs 12 weeks after the operation. The retrieved samples were fixed in 4% paraformaldehyde for 48 hours, decalcified in EDTA for 4 weeks, and cut into slices using a histotome. (**b**) SEM observation of the regenerated bone constructs after 4 and 12 weeks of repair using BAM and PLA scaffolds. Scaled bars: 5µm. **(c)** EDX elemental scanning of the regenerated bone constructs after 12 weeks of repair with BAM (upper) and PLA (bottom) scaffolds.

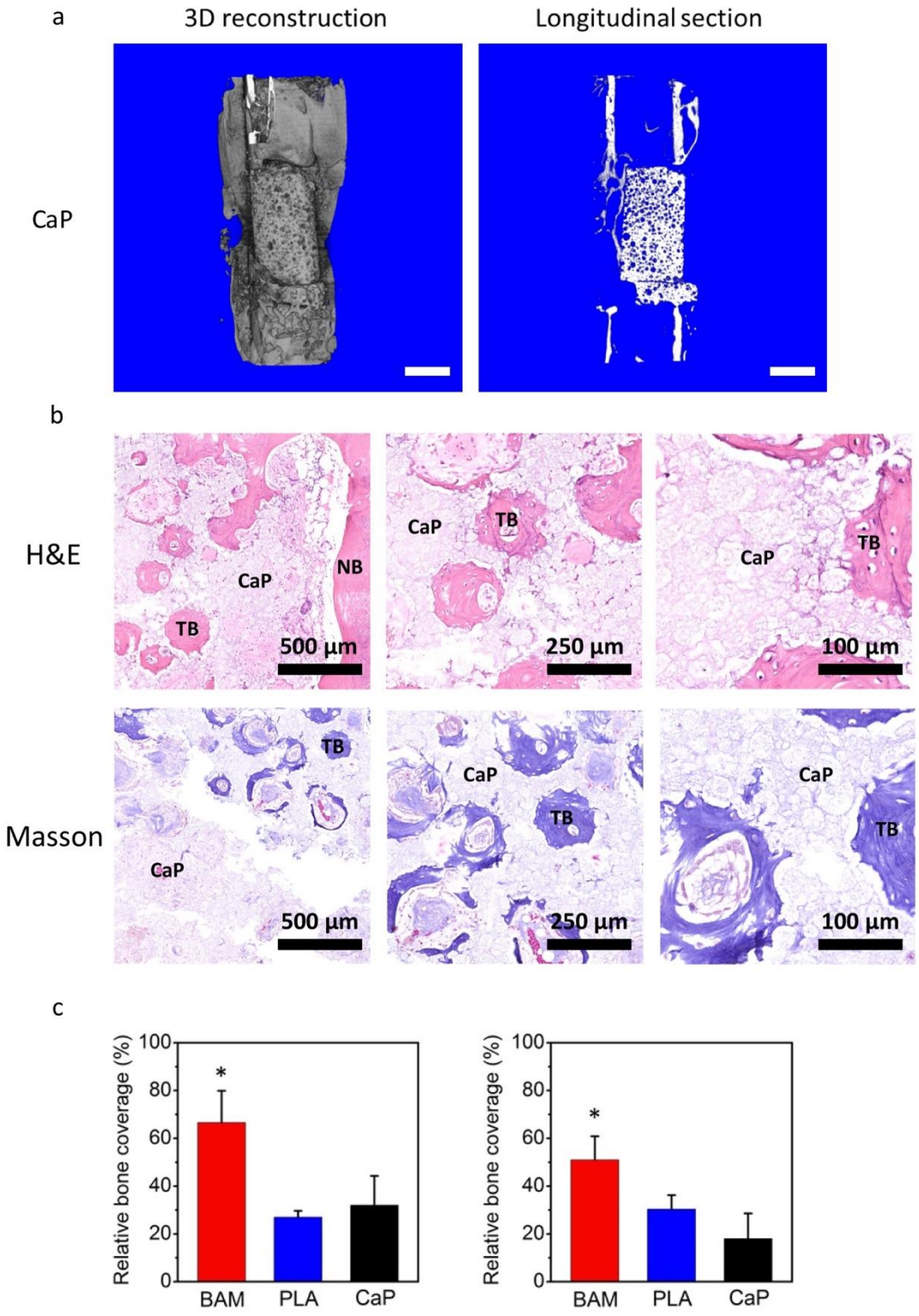

Fig. S12. Micro-CT, histological staining, and quantitative analysis of bone repair in BAM, PLA, and CaP scaffolds. (**a**) Micro CT analysis of retrieved bone in the calcium phosphate (CaP) ceramics scaffolds at 12 weeks postoperatively. 3D reconstruction (left) and longitudinal section profile images (right) showed that the CaP scaffold scarcely degraded with less new bone formation, compared with the BAM scaffold (see Fig. 5b). Scale bar = 5 mm. (**b**) Hematoxylin & eosin (upper) and Masson trichrome (bottom) staining of histological sections for bone ingrowth in the porous CaP scaffold retrieved from rabbit femurs 12 weeks after the operation. The retrieved samples were fixed in paraformaldehyde, decalcified in EDTA for 4 weeks, and cut

into slices using a histotome. Images were captured from areas close to native bone. Both H&E and Masson trichrome staining images showed some new bone regenerated in the scaffold. NB = native bone; TB = tissue engineered bone; CaP = calcium phosphate residual. (**c**) Quantitative analysis on bone repair effect of BAM, PLA and CaP scaffolds. (c1) Relative coverage of regenerated bone in H&E staining images taken from areas close to the native bone, (c2) Relative coverage of regenerated bone in H&E staining images taken from areas away from the native bone. The quantitative data were determined using Image J. $* p < 0.05$, significant differences versus PLA group and vehicle. Results represent means ± standard deviation, $n = 3$ animals per group.

Table S1. XPS quantification for RB/PLA sample retrieved from defect area.

Name	Area (P) CPS.eV	Atomic %	N/C[1]
C1s	105657.84	74.06	**0.10**
N1s	24583.61	7.18	

[1] N/C represent atomic ratio of N to C

Table S2. XPS quantification for RB/BAM sample retrieved from defect area.

Name	Area (P) CPS.eV	Atomic %	N/C[1]
C1s	23764.27	67.84	**0.13**
N1s	12303.57	8.91	

[1] N/C represent atomic ratio of N to C

Table S3. Primer sequences for *Runx-2*, *OCN*, *P2X7*, and *IDH3* genes.

Primer No.	Primer name	Primer sequences（5'-3')	length（bp）
NM_031144	R-β-actin-S	TGCTATGTTGCCCTAGACTTCG	240
	R-β-actin-A	GTTGGCATAGAGGTCTTTACGG	
NM_001278483.1	R-Runx2-S	CAGTATGAGAGTAGGTGTCCCGC	152
	R-Runx2-A	AAGAGGGGTAAGACTGGTCATAGG	
NM_013414.1	R-Bglap-S	GGAGGGCAGTAAGGTGGTGA	148
	R-Bglap-A	GAAGCCAATGTGGTCCGC	
NM_019256.1	R-P2rx7-S	AAGTTAGTACACGGCATCTTCGA	184
	R-P2rx7-A	GTGGGTCCATCCATCCTTTTAT	
NM_031551.1	R-Idh3g-S	ATAACTTGCCACCATCCCACA	287
	R-Idh3g-A	CGTCACTTTCTTACGCCCACT	